Polariton mediated resonant Raman scattering in II–VI microcavities: Exciton lifetime effects

A. Bruchhausen and A. Fainstein*
Centro Atómico Bariloche and Instituto Balseiro, Comisión Nacional de Energía Atómica, 8400 S. C. de Bariloche, Río Negro, Argentina

B. Jusserand
Laboratoire de Photonique et de Nanostructures, CNRS, Route de Nozay, 91460 Marcoussis, France

R. André
Laboratoire de Spectrométrie Physique, Université Joseph Fourier-Grenoble 1, CNRS, Boîte Postale 87, F-38402, St. Martin d'Heres Cedex, France

(Received 23 April 2003; revised manuscript received 5 August 2003; published 24 November 2003)

Semiconductor microcavities enable the study of polariton mediated inelastic light scattering with control of the exciton-photon coupling, and of the exciton and photon strength of the polariton wavefunction. We present a detailed study of the Raman efficiency due to optical phonons resonant with the upper polariton branches in II-VI cavities with embedded CdTe quantum wells. Cavities both in the strong coupling and *very* strong coupling regimes ($\Omega < E_b$ and $\Omega \sim E_b$, respectively) are investigated. In the former, where the mode splitting Ω is smaller than the exciton binding energy E_b, multibranch anticrossings with high order exciton states are observed. The Raman efficiency displays maxima close to the mode anticrossings (zero detuning) decreasing towards the pure excitonic and photonic regimes. This behavior basically reflects the optimization of the polariton coupling to the optical phonons and to exterior continuum photons. A marked steeper Raman efficiency reduction is observed for positive detunings, evidencing the important role of exciton dephasing in the Raman scattering process. Exciton lifetime effects are also apparent in the shape of the multibranch resonance Raman scan, and in the temperature dependence of the Raman efficiency.

DOI: 10.1103/PhysRevB.68.205326 PACS number(s): 78.30.Fs, 42.50.−p, 71.36.+c, 78.66.Hf

I. MOTIVATION

The inelastic scattering of light by optical phonons (Raman scattering) proceeds through the intermediation of electronic excitations. The standard way to describe this process in semiconductor bulk and confined structures (quantum wells, wires, and dots) is as a three step sequence which involves the creation of an interband exciton, the scattering of the latter by the lattice vibration, and finally the recombination accompanied by the emission of the scattered photon.[1] Strictly speaking, however, in highly pure *bulk* semiconductors light does not propagate within the solid as a pure photon but as a combined state involving the oscillating absorption and emission of the photon by an exciton of the same wave vector. The latter combined electromagnetic and matter wave is called a polariton, and is particularly significant for photon energies close to the exciton absorption.[2] Within the polariton point of view the description of the inelastic scattering process is accounted for as the transformation of a photon at the surface of the solid into a polariton of the same energy, the propagation and scattering of the latter within the solid, and the final propagation and conversion of the scattered polariton into an external photon again at the material boundary.[3–5] Basically the main difference in the two descriptions is that, in the latter, the radiation-matter interaction is solved exactly. The Raman cross section, which follows from third order perturbation theory in an excitonic description, thus becomes a first order process in the polariton framework.

Polariton waves, which basically reflect retardation effects in polar excitations, are characterized by a coupled mode energy dispersion that qualitatively differs from that of the pure photon and exciton. This modified dispersion has important consequences in the optical properties of pure bulk semiconductors, which are reflected, e.g., in the light transit time,[6] the reflectance and transmission spectra,[7] and the luminescence line shape.[8] Resonant Brillouin scattering, that is light scattering by acoustical phonons, has proved to be a particularly appropriate technique to derive the polariton dispersion.[7,9] This follows from the linear dispersion of acoustical excitations, which leads to a laser energy dependence of the Brillouin peak shifts. This energy dependence basically maps out the polariton branches.[9] Raman scattering, on the other hand, is essentially different in that the optical excitations are mostly dispersionless. Consequently, the involvement of exciton-polaritons in the light scattering process is more subtly hidden in the resonant Raman peak intensity. It turns out that, in bulk solids, the resonant Raman scans are well described within exciton models that include discrete and continuum states, without the need to rely on polariton effects.[3,10]

The situation is radically different in semiconductor microcavities with embedded quantum wells (QWs).[11,12] In this structures both the QWs excitons and the cavity photon z component of the wave vector are quantized. The wave vector component parallel to the surface ($k_\parallel$) is conserved in the photon transmission into the cavity, implying that any external photon couples to one (and only one) polariton mode of the same $k_\parallel$ and of the same energy. One immediate qualitative difference from bulk materials is that the optical spectra are characterized by a large polariton gap which ranges from $\sim 3-25$ meV in semiconductor microcavities, but which can

 ©2003 The American Physical Society

go up to ~160 meV in organic structures.[13] In addition "additional boundary conditions" (ABCs), essential in bulk,[14] are not required. Most importantly, in microcavities the exciton-photon coupling and both the exciton and photon strengths can be controlled by external parameters or by sample design.

A few papers on resonant Raman scattering (RRS) in semiconductor microcavities have been published to date.[15–19] In Ref. 16 large differences in the angle dependence of the resonant Raman intensity between the polaritonic and pure photonic[15] regimes provided evidence of the involvement of polaritons (as opposed to uncoupled excitons) in the resonant scattering process. Tribe *et al.*,[17] on the other hand, reported ingoing and outgoing single resonant Raman scattering from cavity polaritons. Interestingly, a much weaker resonant enhancement was observed for the upper polariton state as compared to the lower state, indicative of the importance of dephasing in the Raman scattering process. Recently, Stevenson *et al.*[19] reported the observation of uncoupled exciton mediated scattering in microcavities in the strong coupling regime. These three investigations were carried out in III-V semiconductor structures. II-VI cavities are interesting mainly for two reasons. On the one hand, the Rabi gaps and hence the polaritonic effects are much stronger than in GaAs/AlAs based structures. On the other hand, the Raman efficiency for scattering by optical phonons is larger than in III-V materials, allowing clearer Raman studies resonant with strongly luminescent polaritonic states. A preliminary study of the detuning dependence of the Raman intensity in single resonant experiments in such II-VI cavities was reported in Ref. 18.

In this paper we present a detailed investigation of the resonant Raman intensity as a function of cavity photon-exciton detuning in II-VI cavities with different mode splittings. The mode detuning and thus the amount of photon or exciton component in the polariton wave function is varied, exploiting the cavity energy variation in wedged samples. Cavities both in the strong coupling and *very* strong coupling regimes ($\Omega < E_b$ and $\Omega \sim E_b$, respectively) have been investigated. Here Ω is the mode splitting and E_b the exciton binding energy. We show that the Raman efficiency displays maxima close to the mode anticrossings (zero detuning) decreasing towards the pure excitonic and photonic regimes. When $\Omega \sim E_b$, this behavior results in a broad peak in the resonance scan. In addition, a marked decrease of the Raman intensity is observed for positive detunings when the polariton mode approaches the exciton continuum. On the other hand, for $\Omega < E_b$ multibranch anticrossings with higher exciton states are clearly observed in the Raman scans. We present a critical discussion of the available theory of polariton mediated scattering adapted to planar microcavities. The experimental results are analyzed with this model, which provides a qualitative interpretation of the data. One shortcoming of the model is the difficulty of including dephasing and damping in a rigorous way. Several phenomena are analyzed to clarify the role of the polariton lifetime in the scattering process; namely, the Raman efficiency for large positive detunings, the shape and peak position of the resonant Raman scans, and the temperature dependence of the resonant Raman intensity with varying detuning.

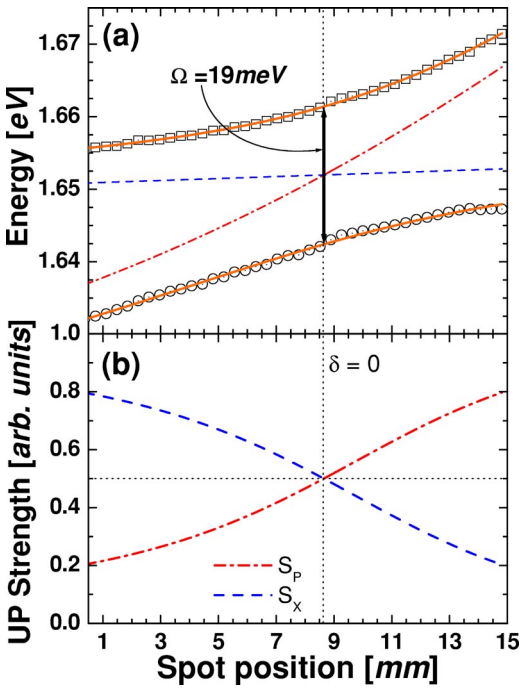

FIG. 1. (a) Sample "A" polariton mode energies at 2.3 K. The solid curve is a fit with the standard two coupled mode model. The Rabi splitting for this sample is $\Omega \sim 19$ meV. (b) Upper mode excitonic (dashed) and photonic (dash dotted) character, derived from the two coupled mode fit.

The paper is organized as follows. In the next section the samples and experimental set-up are presented. Section III provides a survey on the theory of polariton mediated Raman scattering. Section IV, on the other hand, presents the experimental results and is divided into three parts, including data on the very strongly coupled cavity, the observation of multibranch effects in strong coupling, and the Raman efficiency temperature dependence, respectively. Finally, some conclusions and prospects for future work are presented.

II. SAMPLES AND EXPERIMENTAL SET UP

We have studied II-VI microcavities with Rabi splittings ranging from 11 to 19 meV. We will present results on two representative structures. The first sample (A) is a 2λ cavity with three 72 Å CdTe QWs located in each of the four antinodes of the photon field in the $Cd_{0.4}Mg_{0.6}Te$ spacer. The cavity spacer is enclosed by $Cd_{0.4}Mg_{0.6}Te/Cd_{0.75}Mn_{0.25}Te$ Bragg mirrors, 21 pairs on top, and 15.5 on the bottom. A thickness gradient enables a tuning of the cavity mode by displacing the laser spot. This cavity has a relatively large mode splitting of $\Omega \sim 19$ meV. For 72 Å CdTe QWs the exciton binding energy is estimated to be $E_b \sim 20$ meV, and thus this sample is in what is called the "very strong coupling" regime.[20] In Fig. 1(a) we show the polariton modes as a function of laser spot position for this structure, obtained from luminescence measurements at 2.3 K. Note the mode anticrossing and the large Rabi splitting. The latter is so large that the relative separation between the two modes remains

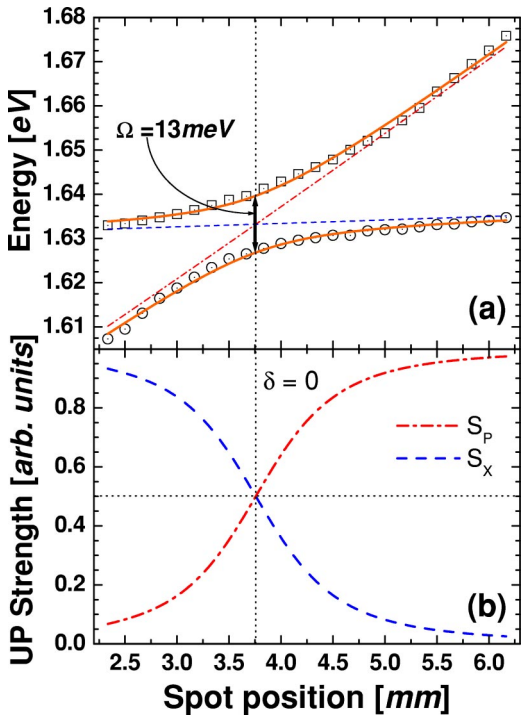

FIG. 2. (a) Sample "B" polariton mode energies at 77 K. The solid curve is a fit with the standard two coupled mode model. The Rabi splitting for this sample is $\Omega \sim 13$ meV. (b) Upper mode excitonic (dashed) and photonic (dashed-dotted) character, derived from the two coupled mode fit.

almost constant for the whole tunable range of the structure. This implies that the photon and exciton strengths of the polariton branches can only be varied in a limited range, as is clear in Fig. 1(b). In this figure we present the photon and exciton components of the upper polariton wave functions deduced from a fit of the polariton energies with a standard coupled mode model. The fit, shown with a continuous line in Fig. 1(a), assumes a parabolic behavior with a spot position for the uncoupled states.

Besides the reduced tunable range of the polariton character in sample A, due to the large Rabi splitting the upper polariton branch overlaps the exciton continuum at relatively small positive detunings. This has critical consequences in the polariton dephasing and damping[20–22] and consequently, as we will show here, also in the Raman efficiency. Sample B was thus designed to have a smaller Rabi splitting by embedding only one group of three CdTe 72 Å QWs in a $\lambda/2$ $Cd_{0.4}Mg_{0.6}Te$ cavity spacer. The Bragg mirrors and thickness gradient are similar to those of sample A. The corresponding mode energies measured at 77 K are shown in Fig. 2(a), together with the two coupled mode fit. The Rabi splitting for this sample is $\Omega \sim 13$ meV. The mode character of the two branches can be varied from almost pure photonic to pure excitonic by changing the detuning, as is shown for the upper branch in Fig. 2(b).

We will report on first order resonant Raman experiments performed at a fixed temperature of 2.3 K as a function of detuning, and as a function of temperature for various values of the detuning. For the lowest temperature the sample holder was immersed in superfluid He to stabilize the temperature and to reduce the laser induced heating. The detuning was varied, changing the laser spot position on the sample surface at almost normal incidence. An almost backscattering configuration was used (that is, light incident and collected in the same direction). A Ti-sapphire laser provided the optical excitation with typical powers below 50 μW, focalized in a spot of ~ 50-μm diameter. Light collection was performed within a fixed cone of $\sim 3°$. This angle corresponds to a relatively small maximum polariton wave vector $k_{\parallel} \sim 4.2 \times 10^3$ cm^{-1}. The collected light was analyzed with a Jobin-Yvon T64000 triple spectrometer operated in subtractive mode and equipped with a liquid-N_2 cooled charge coupled device. The laser energy was tuned for outgoing resonance with the upper polariton branch, as described in Ref. 18. The Raman allowed CdTe QW longitudinal optical (LO) phonons have an energy ~ 171 cm^{-1} (~ 21.2 meV), while the Bragg mirror's stop band have a half-width of approximately ~ 700 cm^{-1}. The backscattering configuration used thus implies that the incoming photons only enter the cavity through the residual transmission of the mirrors ($\sim 0.5\%$), i.e., that the geometry corresponds to *single* outgoing resonance.

III. THEORETICAL BACKGROUND

We begin by briefly introducing the so-called "factorization model" of polariton mediated first order Raman scattering and discussing its extension for photon confined structures. Within the factorization models of polariton-mediated RRS, originally developed for *bulk* semiconductors,[3,5] the Raman efficiency is calculated by *first order* perturbation theory as

$$\sigma_{pol} \propto T_i T_s |\langle \mathbf{K}_i | H_{e-ph} | \mathbf{K}_s \rangle|^2 \rho_s \tau_i . \quad (1)$$

Equation (1) describes a sequential process that involves (*i*) the transmission of an incoming external photon and conversion as a polariton at the sample surface (represented by T_i), followed by the phonon induced scattering of this polariton state ($|\mathbf{K}_i\rangle$) to another ($|\mathbf{K}_s\rangle$) inside the crystal, and terminated by the transmission of the latter to the exterior as a photon where it is detected (T_s). ρ_s is the density of final polariton states, and τ_i is the lifetime of the initial polariton state before it leaves the sample. Although being conceptually simple, this model is limited in that the polariton modes $|\mathbf{K}\rangle$ describe eigenstates of the system and there is no clear and rigorous way to include polariton dephasing and damping.

For the definition of the transmission factors in bulk samples, and because of the existence of more than one polariton branch for energies above the exciton energy, ABCs have to be invoked. This is a complicated procedure, strongly dependent in the model used to describe the excitons and on the surface conditions. In a planar microcavity this problem is not present: only one accessible polariton state exist for a given photon energy and incident photon wave vector $k_{\parallel}$. For the single resonance geometry we are discussing, T_i can be taken as a constant proportional to the Bragg mirror's residual transmission, while T_s is proportional to the photon strength (S_p^s) of the scattered polariton.

On the other, polaritons interact with phonons only through their exciton component. The incoming channel is not in resonance and thus we can assume the matrix element $\langle \mathbf{K}_i | H_{e\text{-}ph} | \mathbf{K}_s \rangle$ to be proportional to the exciton strength (S_x^s) of the scattered, resonantly outgoing, polariton.

The factor ρ describes, within Fermi's golden rule, the number of accessible final states that satisfy the energy conservation condition, $E_s = E_i - \hbar\omega_{ph}$. Here $\hbar\omega_{ph}$ is the energy of the Stokes scattered phonon. In a planar microcavity this has to be replaced by the number of final polariton states with $k_\parallel$ values *subtended by the collection cone*, and satisfying the energy conservation condition. This means that, even for a dispersion that is flat along $k_\parallel$, the number of final states is not infinite but is limited by the collection optics. The density of states is given by $dn/dk = k/2\pi$, and so over the width $\Delta k_\parallel$ around $k=0$ there are $(\Delta k_\parallel)^2/4\pi$ available states/cm^2. Thus, assuming that the collection cone is so small that the polariton energy spread within this $\Delta k_\parallel$ values is smaller than the polariton homogeneous broadening, ρ can be taken as this *detuning independent* constant.

In the literature devoted to polariton mediated scattering in bulk materials, both the transit and dephasing times of the incident polariton are included *ad hoc* in τ_i. For our single outgoing resonance geometry, τ_i can be taken as a constant independent of detuning and determined by the exciton lifetime. This follows from the fact that the incoming laser enters the cavity through the mirror residual transmission, and its energy falls within the exciton continuum. The Raman process incoming vertex is not resonant and is thus not expected to depend strongly on the laser energy. On the other hand, σ_{pol} should also depend on the scattered polariton lifetime τ_s. However, we are not aware of any rigorous and clear way to include this factor within the factorization model.

Summarizing, in this simplified description of polariton mediated first order Raman scattering in microcavities, the Raman efficiency can be taken as $\sigma_{pol} \propto S_p^s S_x^s$.[23] This means that the process is optimized when the detuning is such that the scattered polariton couples best with the exterior continuum photons (i.e., when it is more photonlike) while, at the same time, it couples best with the optical phonons (that is, when it is more excitonlike). Thus a compromise is obtained which predicts a maximum efficiency for zero detuning, decreasing towards the pure exciton and pure photonic limits. Note that our description amounts to saying that the incoming channel is not strongly resonant. This implies that the observed resonant behavior basically reflects the effect of the outgoing (polariton) channel. In what follows we will present the experimental data, using this simple picture as a starting point to describe the involved physics qualitatively.

IV. RESULTS AND DISCUSSION

In Fig. 3(a) we show typical first order Raman spectra corresponding to the CdTe QW optical phonon for a varying laser energy close to outgoing resonance with the upper polariton mode. For these spectra, taken from sample B at 2.3 K, the detuning was constant and $\delta \sim 0$. The Raman intensity

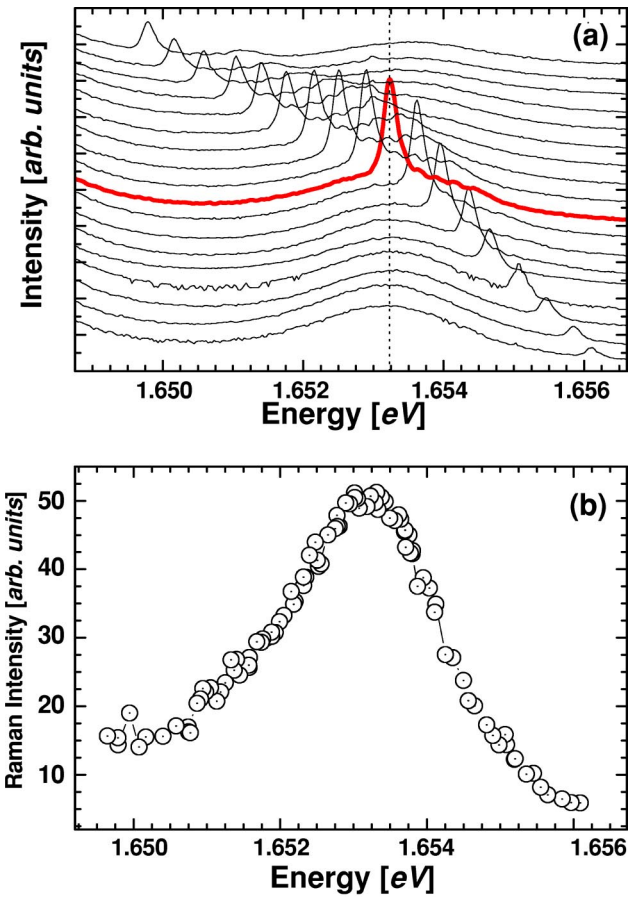

FIG. 3. (a) Typical first order LO-phonon Raman spectra taken for sample B at 2.3 K, for varying laser energy close to outgoing resonance with the upper polariton mode. The detuning is $\delta \sim 0$. The Raman intensity resonates at the upper polariton energy, seen as a broad peak located around 1.6532 eV. The exact resonant spectrum is indicated with a thick solid line. (b) Raman intensity as a function of the Stokes photon energy derived from the data in panel (a).

resonates at the upper polariton energy, seen as a broad peak located around 1.6532 eV (the resonant spectrum is indicated with a thick solid line). The Raman intensity as a function of the Stokes photon energy is displayed in Fig. 3(b). Unfortunately, for reasons not completely understood to date, we have not been able to follow this outgoing resonance through the lower polariton mode. The Raman peak becomes unobservable on top of this latter mode due to the strong luminescence.

Note in the spectra of Fig. 3(a) that, besides the main LO phonon peak, small equidistant oscillations can be observed towards higher energies (i.e., smaller Raman shift). These features, which we believe are associated to confined optical phonons,[24] will be discussed in a forthcoming publication. In this paper we will address the detuning and temperature dependence of the first order LO-phonon intensity in exact resonance with the polariton modes, as shown for $\delta \sim 0$ with the thick solid curve in Fig. 3(a). We begin with the detuning dependence results obtained in the cavity with a large Rabi gap ($\Omega \sim E_b$). We then proceed to discuss the multibranch anticrossings in the sample characterized by $\Omega < E_b$, and we

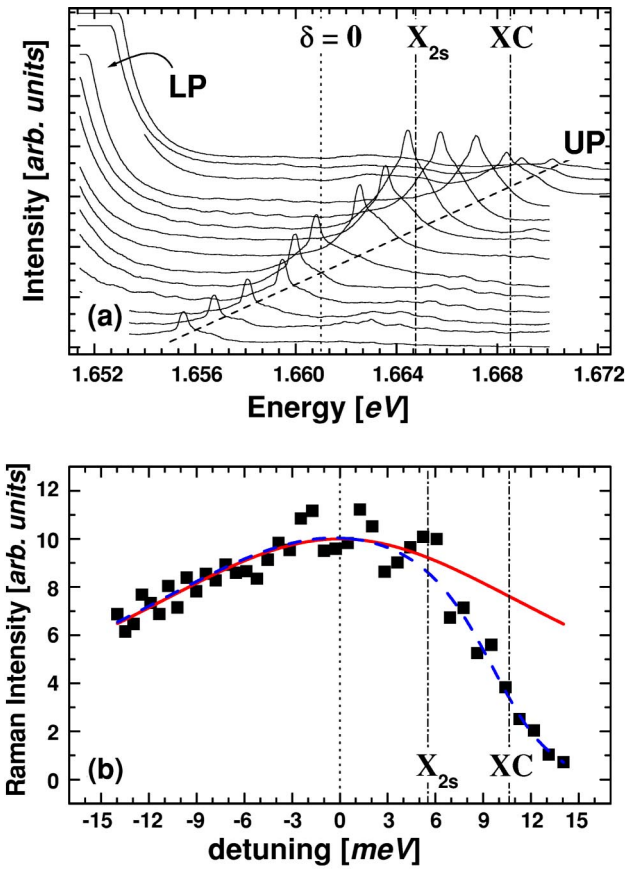

FIG. 4. (a) Raman spectra in outgoing resonance with the upper polariton (UP) taken on sample A at 2.3 K for various values of detuning. LP signals the onset of the lower polariton luminescence peak. X_{2s} (XC) labels higher energy $2s$ (continuum) exciton state. (b) Raman intensity as a function of detuning derived from the data in panel (a). The dashed curve is a guide to the eye. Also shown with a solid curve is the detuning dependence of the Raman efficiency calculated with the factorization model (see the text for details). This curve was obtained using the exciton and photon strengths shown in Fig. 1(a), and scaling the maximum value to fit the data.

finish this section by presenting the temperature dependence of the resonant Raman intensity.

A. RRS detuning dependence: large Rabi gap

In Fig. 4(a) we present resonant Raman spectra taken on sample A for various values of detuning (i.e., spot positions in the sample). Note that this is different to what is displayed in Fig. 3(a), in that here for every spectra (each one corresponding to *different* detunings) the laser energy is varied so that the Stokes (scattered) photon is always in exact resonance with the polariton mode. Several features can be commented from these data: (i) The Raman intensity scan displays a broad maximum around $\delta=0$ [see Fig. 4(b)]. (ii) The polariton mode luminescence also has a maximum but at a different energy that we identify with the first excited exciton state (X_{2s}). No evidence is observed of strong coupling (anticrossing) between the upper polariton and the X_{2s} level in this sample. Note that the excited states have smaller oscillator strengths and larger lifetime broadenings than the X_{1s} level. This explains why strong coupling can be observed for the exciton ground state while being absent for the excited states. (iii) The resonance scan is asymmetric, decreasing more rapidly for positive detunings.

Note that, though weak, the upper polariton [displayed in Fig. 4(a)] can be followed in a large energy region. Its intensity, however, is less than three orders of magnitude weaker than that of the lower polariton. For a peak separation of $\sim$19 meV this would correspond to a carrier temperature $T\sim$30 K. This implies that, at 2.3 K, the carriers are not fully thermalized when they recombine. This agrees with previous reports of thermalization in strongly coupled microcavities (see, e.g., the discussion and references in the paper by Stanley *et al.*).[25]

In Fig. 4(b) we also display with a continuous curve, the detuning dependence of the Raman efficiency calculated with the simple model outlined in Sec. III. This curve was obtained using the exciton and photon strengths shown in Fig. 1(a), and scaling the maximum value to fit the data. Note that the general behavior is well reproduced, and good agreement is obtained for negative detunings. Interestingly, maximum scattering is obtained for $\delta\sim0$ and the Raman efficiency decreases when the exciton energy is approached (negative detuning). This contrasts with nonoptically confined semiconductors, for which the maximum efficiency occurs at the exciton energy. This difference is due to the fact that, in microcavities, polaritons with large exciton character cannot escape efficiently from the cavity. Note, on the other hand, that a clear departure from the model is observed for energies above the X_{2s} level and close to the beginning of the exciton continuum ($XC=X_{1s}+E_b$). This can be due to the additional relaxation channels and to the increased exciton size[20] of the upper polariton when XC is approached in this very strong coupled cavity. This will be discussed in more detail below. Note also that only a modest enhancement is evident in this resonance scan, which displays a rather broad and featureless behavior. This can be explained by the large Rabi splitting and the consequent relatively minor change in the polariton character with varying detuning. In order to be able to modify significantly the polariton character with detuning, we performed experiments similar to the above but on sample B, characterized by a smaller Rabi gap $\Omega\sim$13 meV (see Fig. 2). These results will be presented next.

B. Multibranch polariton mediated RRS

Typical resonant Raman spectra taken at 2.3 K as a function of detuning for sample B are displayed in Fig. 5. For the interpretation of these spectra it is useful to have in mind that, at 2.3 K, the X_{1s} exciton level blueshifts around 10 meV with respect to the 77-K values displayed in Fig. 2(a). Several similarities arise when comparing these spectra with those of sample A [shown in Fig. 4(a)]. First, the Raman intensity displays a maximum and decreases towards the pure excitonic and photonic limits. Second, the polariton luminescence also has a maximum close to the X_{2s} level. However, important differences are apparent. In fact, the observed polariton mode shifts to higher energies but at a certain

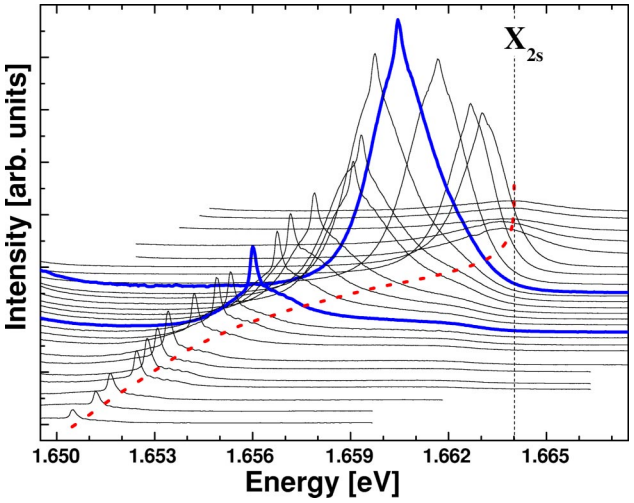

FIG. 5. Raman spectra taken at 2.3 K for sample B, in exact outgoing resonance with the "medium polariton" branch as a function of detuning. The LP observed at lower energies is not shown. Note that at large positive detunings the polariton peak position remains basically fixed in energy at X_{2s}. The two spectra corresponding to maximum Raman intensity (that is, $\delta \sim 0$) are highlighted with thicker curves. Note that the higher energy maximum occurs at energies *below* the X_{2s} level. The Raman intensity for varying detuning obtained from these spectra is displayed in Fig. 6(b). The dashed curve is a guide to the eye. For the interpretation of these spectra it is useful to have in mind that, at 2.3 K, the X_{1s} exciton level shifts to higher energies ~ 10 meV with respect to the 77-K values displayed in Fig. 2(a).

point, though the detuning is continuously varied towards positive values, the peak position remains basically fixed in energy (see the dashed curve in Fig. 5). This evidences an anticrossing of the cavity mode with the X_{2s} level (defined as the high energy saturation value), and thus implies that the observed peak should be assigned to a "medium polariton."[26] The upper branch cannot be clearly distinguished with luminescence measurements at this low temperature (2.3 K). Note, in addition, that the maximum of the Raman efficiency and of the mode luminescence occurs clearly *below* the X_{2s} energy. We recall from Sec. III that the maximum Raman efficiency in a polariton mediated Raman resonance scan occurs for zero detuning, and not at the exciton energy. This provides further consistency to the description of the observed behavior as a three level (X_{1s}, X_{2s}, and the cavity mode) anticrossing. We recall here that, for sample A, the anticrossing with the X_{2s} state was absent at 2.3 K. This can be interpreted as due to a larger lifetime broadening in sample A, as compared to sample B, originated in the stronger disorder expectable in a 2λ cavity with many more QWs. In any case, note that at 77 K in sample B the anticrossing with the X_{2s} level is also washed out by temperature induced lifetime broadening effects [see Fig. 2(a)].

In Fig. 6 we present with full circles the energy difference between the medium (MP) and lower (LP) polaritons (top panel), together with the Raman intensity as a function of the medium polariton mode energy (bottom panel) derived from the spectra of Fig. 5. Several notable features can be high-

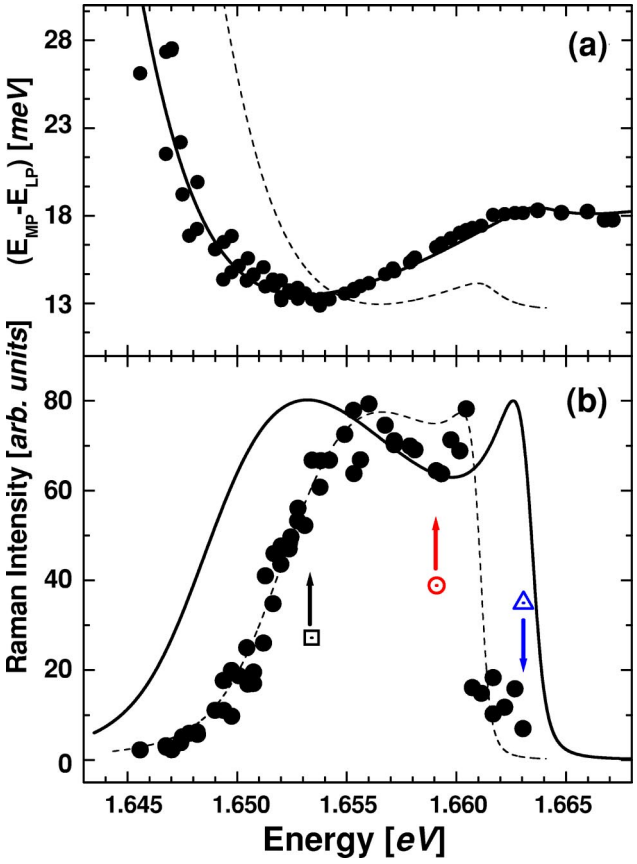

FIG. 6. (a) The energy difference between the medium (MP) and lower (LP) polaritons for sample B is shown with full circles. (b) Raman intensity as a function of the medium polariton mode energy. Both the energy difference (a) and the Raman intensity (b) are derived from the spectra displayed in Fig. 5. The solid and dashed curves in (a) and (b) were obtained using the three coupled mode model. The solid curve was obtained by fitting the polariton energies $E_{MP}-E_{LP}$. The dashed curve, on the other hand corresponds to the same model parameterized to better fit the resonant Raman scan. In both cases, we used $\beta=0$ (see the text for details). The arrows in panel (b) label the values of detuning for which the temperature dependence is reported.

lighted from these curves: (i) The general behavior of the resonance Raman scan is similar to that presented for sample A in Fig. 4. However, the magnitude of the Raman intensity variation is much larger than that observed for sample A. Note that the Raman peak becomes unobservable for large detunings. This is consistent with the more marked variation of S_p and S_x in this sample. (ii) On the other hand, the Raman intensity scan does not display a single peak but two clear maxima. The two peaks do not have the same width, being broader the lower energy one. (iii) We observe that this latter maximum does not coincide with the minimum of $(E_{MP}-E_{LP})$ (which corresponds closely to $\delta=0$ between the cavity mode and X_{1s}) but is clearly blueshifted.

In order to describe the observed behavior we extend the above presented theory to include three coupled modes. In this case, the scattered polariton state is given by $|K_s\rangle = a_p|1_p,0_{X_{1s}},0_{X_{2s}}\rangle + a_{X_{1s}}|0_p,1_{X_{1s}},0_{X_{2s}}\rangle + a_{X_{2s}}|0_p,0_{X_{1s}},1_{X_{2s}}\rangle$, where, e.g., $|1_p,0_{X_{1s}},0_{X_{2s}}\rangle$ indicates the state involving one

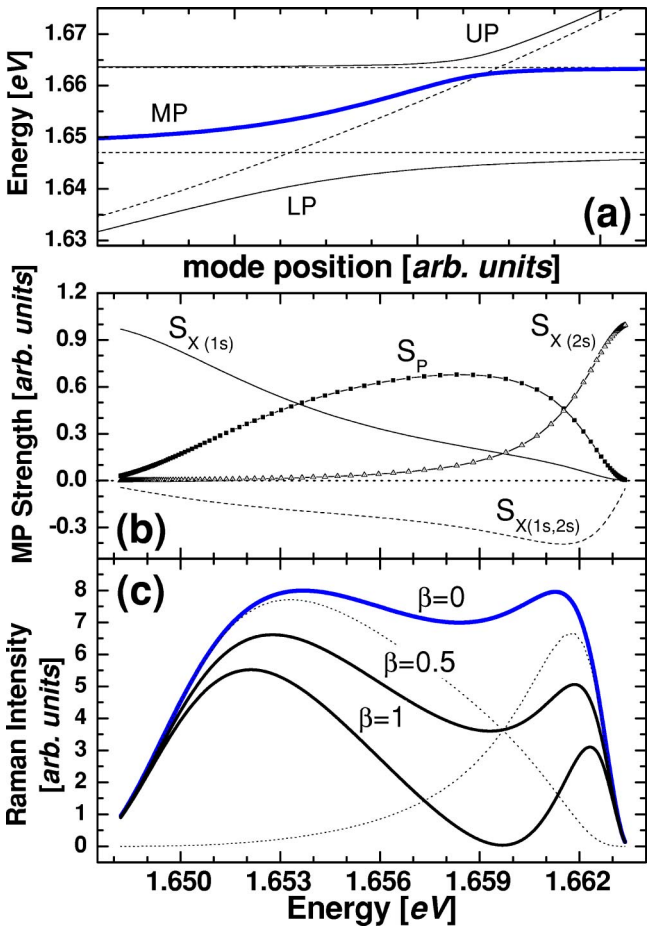

FIG. 7. (a) Calculated polariton modes in the case of three strongly coupled states (sample B). The medium polariton branch, for which the outgoing Raman resonance scan is studied, is highlighted with a thick solid curve. In panels (b) and (c) we show, respectively, the deduced photonic and exciton strengths of the medium polariton state, and the corresponding Raman efficiency calculated according to Eq. (2). Curves for various values of coherence factor β are given. The dotted curves in (c) represent the independent contribution of each exciton level to the resonant Raman efficiency (i.e., $S_p S_{X_{1s}}$ and $S_p S_{X_{2s}}$). On the other hand, $S_{X_{1s,2s}}$ in (b) describes the interference term (see the text for details).

cavity photon and no excitons, and the coefficients a_l give the (detuning dependent) photon or exciton weight of the polariton state. Expressed in terms of this final state, the Raman efficiency can be written as

$$\sigma_{pol} \propto S_p |a_{X_{1s}} + a_{X_{2s}}|^2 \propto S_p (S_{X_{1s}} + S_{X_{2s}} + \beta S_{X_{1s,2s}}), \quad (2)$$

where the photon or exciton strengths are given by $S_l = |a_l|^2$, and $S_{X_{1s,2s}} = a^*_{X_{1s}} a_{X_{2s}} + a_{X_{1s}} a^*_{X_{2s}}$ is the interference term. The coherence factor β is introduced in the assumption of only partial coherence between the polarizations associated with the two intervening excitonic levels.[27] For simplicity, in Eq. (2) we assume the same coupling between the optical phonons and the two involved exciton states.

In Fig. 7(a) we show the calculated polariton modes in the case of three strongly coupled states. For this figure we have used the experimental values for the uncoupled X_{1s} and X_{2s} energy levels, for the X_{1s} Rabi splitting, and for the spot position dependence of the cavity mode (sample B). The Rabi splitting for the X_{2s} level, on the other hand, was taken as $\Omega_{2s} = 2.5$ meV to better fit the shape of the resonant Raman scan (see below). This value is consistent, on the other hand, with the fact that no anticrossing is observed with the X_{2s} level at 77 K (see Fig. 2). The medium polariton branch, for which the outgoing Raman resonance scan is displayed in Figs. 5 and 6, is highlighted with a thick solid curve. In panels (b) and (c) we show, respectively, the deduced photonic and exciton strengths of the medium polariton state, and the corresponding Raman efficiency calculated according to Eq. (2). On the other hand, $S_{X_{1s,2s}}$ in panel (b) corresponds to the above described interference term. The dotted curves in Fig. 7(c) represent the independent contribution of each exciton level to the resonant Raman efficiency (i.e., $S_p S_{X_{1s}}$ and $S_p S_{X_{2s}}$).

Let us first consider the ''ideal'' case, $\beta = 1$. The energies for which S_p intersects the excitonic strengths $S_{X_{1s}}$ and $S_{X_{2s}}$ correspond to an almost optimized scattering efficiency and thus to maxima (two in this case) in the resonant Raman scan. Since in each crossing the exciton strength of the third (not involved) state is relatively small, the energies of the maxima basically coincide with the intersections. However, note that if X_{1s} and X_{2s} were closer in energy, or their corresponding Rabi splittings were larger, the resonant Raman scan maxima would not necessarily be given by the conditions $S_p = S_{X_{1s}}$ and $S_p = S_{X_{2s}}$. Also note that the effect of the interference between X_{1s} and X_{2s} is quite strong. In fact, $a_{X_{1s}}$ and $a_{X_{2s}}$ have different signs and can cancel each other, leading to a zero and clearly separated maxima in the Raman efficiency. Moreover, the interference leads to a slightly augmented separation between the two Raman maxima. The calculated Raman efficiency shown in Fig. 7(c) ($\beta = 1$) qualitatively describes the main features of the experimental results. This includes the existence of two peaks in the resonance scan, and their contrasting widths derived from the markedly different Rabi splittings associated with each of the two exciton levels. Note the related abrupt decay of the Raman signal in the high energy tail, coincident with what is observed experimentally.

However, two important differences between the calculated and experimental curves are apparent. First, the maxima in the experimental Raman intensity are only weakly defined; the Raman scan clearly does not go through a cancellation as shown for $\beta = 1$ in Fig. 7(c). A comparison with the experimental data suggests that, in our experiments, the contributions due to X_{1s} and X_{2s} are mostly incoherent.[27] In fact, we have verified that the best fit using the proposed model is obtained with $\beta \sim 0$. Second, the calculated separation between the maxima (~ 10 meV) is markedly larger than that observed experimentally (~ 5 meV). A quantitative test with the data shows clear shortcomings of the model. In Fig. 6 we show, with a solid curve, the theoretical Raman efficiency obtained by fitting ($E_{MP} - E_{LP}$) and deriving from this fit the exciton and photon strengths of the medium po-

lariton branch. Although the general shape of the resonance scan is basically well reproduced, the position of the maxima are not described appropriately. Note in Fig. 7(c) that the coupling to a third mode with the assumption of complete incoherence ($\beta=0$) leads to a slight reduction of the separation between resonance maxima. However, though this effect goes in the right direction it is included in the calculation shown in Fig. 6 and is clearly not able to reproduce the strong shift of the peaks.

In Fig. 6(b) we also show a calculated curve with parameters chosen so as to best describe the measured resonant Raman scan (dashed curve). This curve was obtained using $\beta=0$. The deduced polariton mode separation ($E_{MP}-E_{LP}$) is also shown in Fig. 6(a) with a dashed curve. Note that the Raman scan can be reasonably well reproduced, but only by using unrealistic values for ($E_{MP}-E_{LP}$). In fact, for these curves we had to shift the X_{1s} level to higher energies by ~ 2 meV, and reduce the $X_{1s}-X_{2s}$ separation to ~ 11 meV. This latter value, besides being in contrast with the observed luminescence peak positions, is ~ 3 meV too small compared to the values found in the literature for QWs of similar width.

We believe that the observed behavior might be related to lifetime effects on the Raman efficiency. In fact, if the medium polariton lifetime is mainly determined by exciton dephasing (τ_X) and not by the cavity photon lifetime (τ_p), it is to be expected that maximum Raman efficiency will be obtained not for $\delta=0$ (i.e., for $S_p=S_X$) but for a polariton state with a detuning such that $S_p>S_x$ (predominant photonic character), since in this case the corresponding polariton lifetime will be larger. That is, from this handwaving argument and the polariton strengths displayed in panel (b) of Fig. 6, we foresee that the effect of having $\tau_X<\tau_p$ will be to reduce the Raman scan peak separation. This is in agreement with the experiment. Note that our interpretation is conceptually similar to the ''cavity pulling'' effect proposed by Stanley *et al.*[25] In fact, as reported in this latter work, the maximum photoluminescence intensity is observed away from resonance and, in addition, it is the photonlike line that displays the most intense luminescence. As we discussed in Sec. III, exciton lifetime effects are also apparent in the positive detuning dependence of the resonance scan. In Sec. IV C further proof of the central role of exciton dephasing in the inelastic light scattering process will be derived from the temperature dependence of the Raman efficiency.

C. RRS temperature dependence

In the previous sections we argued about the importance of exciton lifetime effects to appropriately account for the observed shape of the resonance Raman scans, namely, the rapid decay of the Raman efficiency at positive detunings (see Fig. 4) and the peak positions in multibranch polariton resonance Raman scans (see Fig. 6). We recall that two different mechanisms that can reduce the Raman efficiency come into play as the polariton branch approaches the continuum exciton states, that is, the exciton additional relaxation channels[17] and the increased exciton size in the polariton state.[20] The latter basically reflects the fact that the exciton state is no more stable as the polariton branch overlaps the exciton continuum.[20] It can affect the Raman efficiency both through a reduction of the oscillator strength and by limiting the polariton lifetime. On the other hand, this polariton lifetime is clearly affected when higher energy states become available as final states for polariton scattering processes. In fact, at finite temperatures the interaction with acoustic phonons can induce the scattering of the polariton modes to the discrete and continuum exciton states lying at higher energies. This limits the polariton lifetime and consequently also the Raman efficiency. The importance of this mechanism can be tested by performing resonant Raman experiments at different temperatures and for various polariton energies. This is shown in Fig. 8 for sample B, and for three values of the polariton energy (i.e., detuning), indicated with arrows and labels in Fig. 6. In these experiments, and since both the exciton and cavity mode energies depend on temperature, the laser energy and spot position were tuned at each temperature so as to maintain the separation between the lower and medium polaritons constant. This is equivalent to keeping unaltered the exciton and photonic strength of the studied polariton branch. The temperature given is nominal for the sample holder and is not corrected for possible heating at the laser spot. At higher temperatures the measurements are hampered by the strong increase of the luminescence.

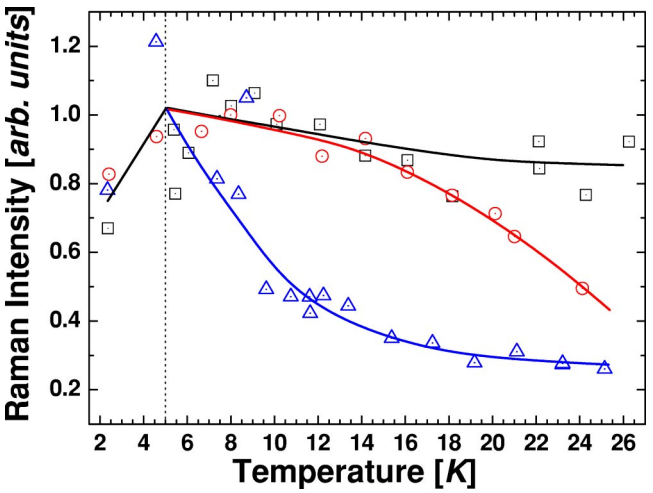

FIG. 8. Temperature dependence of the outgoing resonant Raman intensity (sample B) for three values of the polariton energy (i.e, detuning). The corresponding energies are indicated with arrows in Fig. 6. In these experiments, and since both the exciton and cavity mode energies depend on temperature, the laser energy and spot position were tuned at each temperature so as to maintain the separation between the lower and medium polaritons constant. The solid curves are guides to the eye.

The following features can be noted from Fig 8: (i) a weak but systematic rise is observed for the three presented detunings between 2 and ~ 4 K. We do not have to date an explanation for this rather peculiar behavior. (ii) Above ~ 4 K and up to ~ 30 K for $\delta\sim 0$ (labeled with open squares) the Raman intensity remains almost constant with only a smooth decay. For this value of the polariton energy and for the measured temperatures the only higher energy

final accessible states belong to the same polariton branch. (iii) At the highest studied polariton energy (open triangles) the Raman efficiency displays a rapid decay with temperature being almost completely quenched at ~ 20 K. This result is consistent with the fact that, for this polariton energy, the higher exciton states and the exciton continuum lie at only 3–5 meV. (iv) The behavior for the intermediate detuning falls between these two limits. These results demonstrate that the opening of new relaxation channels for the exciton component of the polariton modes is determinant of the polariton lifetime, and that the latter strongly affects the Raman efficiency. A theory of polariton mediated Raman scattering in microcavities that includes these effects might be useful to distinguish between lifetime and exciton size effects in experiments like those reported in this work.

V. CONCLUSIONS

In conclusion, we have presented a detailed study of polariton mediated Raman scattering in II-VI cavities with embedded CdTe QWs. We have analyzed the data through the factorization model adapted from bulk materials to photon confined structures. This model predicts the observation of Raman scan peaks close to zero detuning, in agreement with what is observed experimentally. These peaks basically reflect that polariton mediated Raman scattering by phonons requires to maximize, at the same time, the excitonic and photonic strengths. However, though the proposed theory qualitatively describes the general behavior and number of maxima in the resonance Raman scans, it cannot account for several important features. These include (i) the steeper decay of the Raman efficiency for positive detunings, (ii) the markedly reduced separation of the Raman maxima in the multibranch situation, and (iii) the detuning dependent decay of the Raman efficiency with temperature. These results strongly indicate that a polariton mediated Raman theory is required that includes, in a rigorous way, both polariton lifetime effects and the increased exciton size at positive detunings in semiconductor microcavities. We believe that the inelastic scattering of light in optically confined microcavities, where polaritons define the way in which light interacts with matter, remains a fundamental, interesting, and basically unexplored subject.

ACKNOWLEDGMENT

We would like to acknowledge the collaboration of Mariano Trigo in the initial stages of this investigation.

*Also at CONICET, Argentina. Electronic address: afains@cab.cnea.gov.ar

[1] For a comprehensive review of resonant Raman scattering see M. Cardona, in *Light Scattering in Solids II*, edited by M. Cardona and G. Güntherodt (Springer, Heidelberg, 1989).

[2] J.J. Hopfield, Phys. Rev. **182**, 945 (1969).

[3] B. Bendow and J.L. Birman, Phys. Rev. B **1**, 1678 (1970); B. Bendow, *ibid.* **2**, 5051 (1970).

[4] R. Zeyher, Chin-Sen Ting, and J.L. Birman, Phys. Rev. B **10**, 1725 (1974).

[5] M. Matsushita, J. Wicksted, and H.Z. Cummins, Phys. Rev. B **29**, 3362 (1984); M. Matsushita and M. Nakayama, *ibid.* **30**, 2074 (1984).

[6] M. Nawrocki, R. Planel, and Benoît à la Guillaume, Phys. Rev. Lett. **36**, 1343 (1976).

[7] C. Weisbuch and R. G. Ulbrich, in *Light Scattering in Solids III*, edited by M. Cardona and G. Güntherodt (Springer, Berlin, 1989); also see V.A. Kisilev, B.S. Razbirin, and I.N. Uraltsev, Phys. Status Solidi B **72**, 161 (1975).

[8] F. Ashary and P. Yu, Solid State Commun. **47**, 241 (1983).

[9] R.G. Ulbrich and C. Weisbuch, Phys. Rev. Lett. **38**, 865 (1977); J. Wicksted, M. Matsushita, H.Z. Cummins, T. Shigenari, and X.Z. Lu, Phys. Rev. B **29**, 3350 (1984).

[10] A. Nakamura and C. Weisbuch, Solid State Commun. **32**, 301 (1979).

[11] *Confined Electrons and Photons: New Physics and Applications*, edited by E. Burstein and C. Weisbuch (Plenum, New York, 1995).

[12] M.S. Skolnick, T.A. Fisher, and D.M. Whittaker, Semicond. Sci. Technol. **13**, 645 (1998).

[13] A.I. Tartakovskii, M. Emam-Ismail, D.G. Lidzey, M.S. Skolnick, D.D.C. Bradley, S. Walker, and V.M. Agranovich, Phys. Rev. B **63**, 121302(R) (2001).

[14] R. Zeyher, J.L. Birman, and W. Brenig, Phys. Rev. B **6**, 4613 (1972).

[15] A. Fainstein, B. Jusserand, and V. Thierry-Mieg, Phys. Rev. Lett. **75**, 3764 (1995).

[16] A. Fainstein, B. Jusserand, and V. Thierry-Mieg, Phys. Rev. Lett. **78**, 1576 (1997).

[17] W.R. Tribe, D. Baxter, M.S. Skolnick, D.J. Mowbray, T.A. Fisher, and J.S. Roberts, Phys. Rev. B **56**, 12 429 (1997).

[18] A. Fainstein, B. Jusserand, and R. André, Phys. Rev. B **57**, R9439 (1998).

[19] R.M. Stevenson, V.N. Astratov, M.S. Skolnick, J.S. Roberts, and G. Hill, Phys. Rev. B **67**, 081301(R) (2003).

[20] J.B. Khurgin, Solid State Commun. **117**, 307 (2001).

[21] J. Bloch, T. Freixanet, J.Y. Marzin, V. Thierry-Mieg, and R. Planel, Appl. Phys. Lett. **73**, 1694 (1998).

[22] H. Deng, G. Weihs, C. Santori, J. Bloch, and Y. Yamamoto, Science **298**, 199 (2002).

[23] In Ref. 18 we arrive at this same expression but based on wrong assumptions for the final density of states and for the polariton escape time appearing in Eq. (1).

[24] A.J. Shields, M.P. Chamberlain, M. Cardona, and K. Eberl, Phys. Rev. B **51**, 17 728 (1995).

[25] R.P. Stanley, R. Houdré, C. Weisbuch, U. Oesterle, and M. Ilegems, Phys. Rev. B **53**, 10 995 (1996).

[26] Three mode anticrossings involving the cavity confined photons and the X_{1s} and X_{2s} states have been observed in II-VI cavities using reflectivity measurements. See, e.g., Frederic Boeuf, Ph.D. thesis, Université Joseph Fourier-Grenoble 1, 2000.

[27] The coherence factor basically defines whether the contributions

from X_{1s} and X_{2s} must be added before or after squaring in the Raman efficiency. A description similar to the one presented here has been discussed by J. Menéndez and M. Cardona, Phys. Rev. Lett. **51**, 1297 (1983), to account for the interference between allowed and forbidden Raman scattering by LO phonons in bulk GaAs. Impurity induced scattering is expected to be incoherent. As we will discuss in a forthcoming publication, we believe that the oscillations observed in the first order Raman spectra in Fig. 3 indicate that disorder is active as intermediate state in the scattering process.